ö Biointerphases
a SpringerOpen Journal

ORIGINAL ARTICLE
Open Access

Diffusion and interaction in PEG-DA hydrogels

Valentin Hagel[1,3], Tamás Haraszti[1,3] and Heike Boehm[1,2,3]*

Abstract
Polyethylenglycol (PEG) hydrogels are widely used as tuneable substrates for biological and technical applications due to their good biocompatibility and their high hydrophilicity. Here we compare the mesh size and diffusion characteristics of PEG hydrogels by analyzing the diffusion of solutes with different, well-defined sizes over long and short time scales. Interestingly, one can tune the mesh size and the density of the gel simply by changing the inital concentrations of the PEG-diacrylate (PEG-DA) polymer, which also enhances the solute uptake in equilibrium through the interaction with the PEG chains. This increased uptake can be characterized by an enhancement factor determined by partition ratio analysis. It increases linearly with the polymer volume fraction, but is not caused by immobilization inside the hydrogel as evident from FRAP measurements, thus rendering these hydrogels ideal materials for i.e. drug delivery applications.

Background

Hydrogels are water-swollen, cross-linked polymeric materials with a complex specific three-dimensional architecture. In the last decades they have gained considerable attention due to their applicability both as biological and as technical building blocks. In technical applications, hydrogels serve as basic building blocks for gel electrophoresis or size exclusion chromatography, etc. Moreover they are nowadays implementet as "intelligent" chemo-mechanical materials using them as stimuli-responsive sensor-actor systems [1] based on their high sensitivity to environmental conditions [2] such as pH [3,4], temperature [5], solvent composition [3], light or pressure [2]. In biological contexts, hydrogels have become ideal model systems for tissue matrices due to their similarity to the extra-cellular matrix (ECM). They opened up new methods to study cell behavior such as migration on substrates with different stiffness [6] as well as in three dimensions [7]. Understanding the permability to various solutes such as growth factors, vitamins, etc. in these synthetic ECMs [8] not only enhances our basic understanding of ECMs, but can also be employed in

various biomedical applications including the use of hydogels as drug- and cell carriers, artificial tissue scaffolds or growth factor release systems [9].

Therefore, understanding diffusion processes of macromolecules in hydrogel-based systems plays a key role in the design of new hydrogel-based materials. Controlling and predicting diffusion within biomedical materials, such as artificial implants or drug delivery systems, is a prerequisite for the design of feasible materials. However, diffusion within hydrogels is a very complex process due to the different interactions a molecule undergoes while diffusing through the hydrogel mesh. The physical models of diffusion are mainly based on either hydrodynamic effects, obstruction effects, the free volume theory or, in further advanced cases, on thermodynamic models [10]. Many of these models successfully describe diffusion processes under various circumstances and thus promote the understanding the complex diffusion properties within hydrogels. However, many controversies still remain and it seems that obstruction effects, hydrodynamic interactions and thermodynamic agitation should all be considered simultaneously in order to develop a broader understanding of diffusion in polymeric networks [10]. The limited ability of diffusion models to describe diffusion processes in a broad range of experimental situations is due to the many types of possible specific interactions between the polymer mesh and the diffusing species [11]. Such interactions include hydrogen bonding, electrostatic and van der Waals interactions as well as hydrophobic effects. Also, the influence of altered solvent properties such as

*Correspondence: boehm@is.mpg.de
[1]Department of New Materials and Biosystems, Max Planck Institute for Intelligent Systems Heisenbergstr. 3, 70569 Stuttgart, Germany
[2]CSF Biomaterials and Cellular Biophysics, Max Planck Institute for Intelligent Systems Heisenbergstr. 3, 70569 Stuttgart, Germany
Full list of author information is available at the end of the article

Springer

structuring of solvent molecules by the polymer mesh expressed as an entropic effect [12] or as an increased 'local viscosity' of the solvent [13] are difficult to be incorporated quantitatively to construct exact diffusion models.

Among the synthetic hydrogels, polyethylene glycol (PEG) hydrogels belong to the most important materials. As they exhibit many advantageous material properties such as being transparent, deformable, biocompatible [14], and permeable to gases and nutrients [15], PEG hydrogels are widely used in biomedical applications including artificial tissue scaffolds, matrices for the controlled release of biomolecules [14], wound dressings [16], and contact lenses [17]. Thus, understanding diffusion mechanisms within PEG hydrogels and understanding them with respect to the polymeric structure is of great interest.

In this work we used monodisperse, fluorescent dextrans of various hydrodynamic radii, to study diffusion within PEG hydrogels of different densities. Dextrans are branched, spherical polysaccharides of predefined controlled size widely used as neutral model diffusants [18-20]. Diffusion coefficients were measured using the fluorescence recovery after photobleaching (FRAP) on a setup which has been established for three-dimensional measurements in hydrogel samples. Furthermore, the detailed analysis of the equilibrium partition ratios is fundamental in understanding the physical-chemical nature of the interaction between solutes and polymer [21]. Complementing the FRAP analysis with partitioning analysis provides access to short and long term interactions separately. Further, partitioning analysis allows to probe the real mesh size of the hydrogels and to investigate their polymeric microstructure. Mesh sizes are also calculated based on the measurement of shear moduli and using the theory of rubber elasticity and compared with the outcome of the partitioning analysis.

Results and discussion

We characterized the permeability of biocompatible polyethylenglycol(PEG) hydrogels based on their mechanical properties as well as on the diffusion behavior of fluorescent dextranes over long and short time frames. First we synthesized three different PEG hydrogels based on the same PEG-DA (20 *kDa*) precursor molecules but with different polymer densities. To this end, we added the same amount of initiator to solutions of PEG-DA at 10, 20 and 30% (v/v). The different concentrations of PEG-DA during the radical polymerization reaction lead to different numbers of cross-links within the hydrogel and therefore different rheological properties such as their swelling behavior. For each hydrogel the volumetric swelling ratio (Q) was determined after equilibration in PBS in comparison to the initial polymer volume. Their polymer volume

fraction ϕ is then given by the inverse of the swelling ratio (Table 1). Varying PEG density in this fashion, the elastic moduli of the hydrogel can easily be tuned. Here, the shear moduli G of the hydrogels vary from 2.8 kPa for hydrogels with the lowest polymer volume fraction of 0.03 up to 13.7 kPa for the more dense hydrogels with a polymer volume fraction of 0.08 (Table 1).

We assume that the difference in densities also affects the permeability of the hydrogels. Therefore we employed two different techniques to determine the mesh size and the diffusion characteristics inside the hydrogels and compared these results with the mesh size calculation based on the elastic modulus of the hydrogel. For both methods we prepared several hydrogels which were each incubated in a solution of monodisperse fluorescently labeled dextran molecules. Allowing five days of diffusion to reach equilibrium, the difference in the fluorescence intensity to the bulk solution depends on the size of the applied dextran as well as the mesh sizes ξ of the hydrogel (Figure 1). The relation between the two intensities is given by the partition ratio K. Further information on the network structure of the hydrogels were obtained by analyzing the decay curve of the partition ratios as a function of the radius of the test solutes [21]. Fitting analysis of the obtained data clearly indicate that the partition ratios follow an exponential decay represented by the form

$$K = A \cdot exp\left(-s(r_h + r_f)\right) \tag{1}$$

where r_h represents the hydrodynamic radius of the test molecules, r_f the cross-sectional fiber radius of the PEG chains and A is a numeric factor. For $A = 1$ equation (1) describes the theoretically expected form of the partition ratios of spherical, non-interacting molecules in a network of randomly oriented planes [21]. In this case the factor s represents the mean surface area of the network planes per unit volume (see Appendix). Deviation from ideal partitioning is described by the enhancement (or exclusion) factor E [22], which is directly related to the partition ratio of point solutes corresponding to $K_0 = A \cdot exp\left(-s \cdot r_f\right)$. Ideally, the partition ratio for a point solute reduces to the volume fraction of water in the gel: $K_0 = 1 - \phi$. Therefore

Table 1 Charakteristica of the three different PEG-DA (20kDa) hydogels depending on the PEG-DA concentration in the preparation mixture

% PEG-DA (v/v)	Swelling ratio Q	Polymer volume fraction ϕ[10^{-2}]	Shear moduli G [kPa] at 25°C
10	32.67 ± 0.73	3.06 ± 0.07	2.8 ± 0.7
20	19.06 ± 0.41	5.25 ± 0.12	7.7 ± 0.7
30	13.20 ± 0.33	7.58 ± 0.20	13.7 ± 0.7

Errors correspond to standard deviations of triplicates.
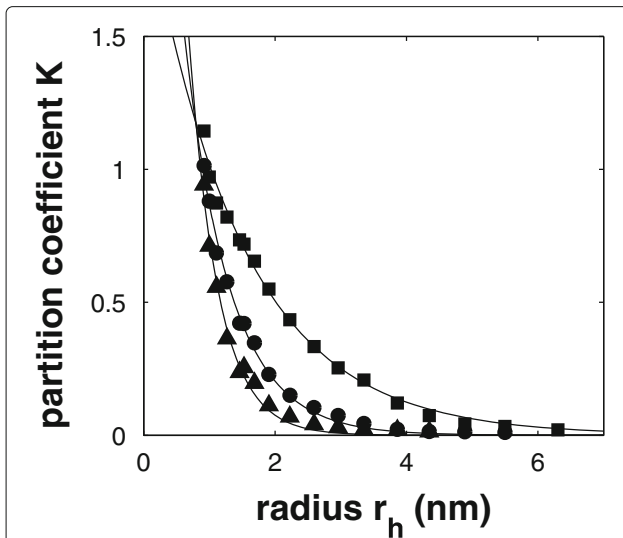
Figure 1 The partition ratio *K* of monodisperse FITC-dextrans depends on the size of dextrans and the polymer density of the PEG hydrogel represented by the polymer volume fraction $\phi = 0.03$ (squares), 0.05 (circles) and 0.08 (triangles). Exponential decays correspond to fits to equation 1, where r_h represents the hydrodynamic radius of the dextran molecules and r_f the fiber radius of 0.51 nm. Error bars not visible.
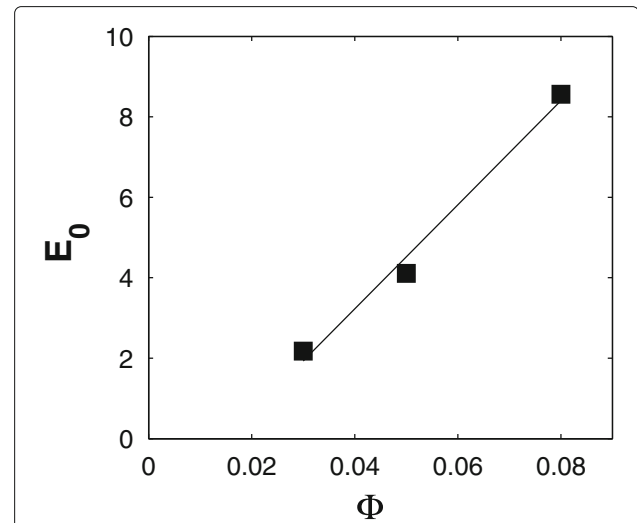
Figure 2 The enhancement factor *E* scales linearly with the volume fraction ϕ for PEG hydrogels.

the enhancement factor $E \equiv K_0/(1 - \phi)$ can be described as

$$E \equiv \frac{A \cdot exp\left(-s \cdot r_f\right)}{(1 - \phi)}.\qquad(2)$$

We used the results from the fitting analysis to calculate the enhancement factor *E* for point solutes. In our PEG hydrogel, *E* is larger than unity and scales linearly with the volume fraction ϕ (Figure 2) indicating a significant interaction with the polymer backbone [22]. The increase of *E* also suggests, that mesh sizes calculated based on fitting equation (2) will result in an overestimated *s* value, and an underestimation of the mesh size of the hydrogel.

From the fitting parameter *s* it is possible to calculate the mean distance *d* between neighboring knots of the polymer network corresponding to the average mesh size $< \xi >$ using the relation $< \xi > = 3/s$ thereby allowing to estimate the mesh sizes of the hydrogels. The measured values of the average mesh sizes $< \xi >$ based on the partition ratio correspond well to values calculated based on the swelling ratio and the elastic modulus (Table 2). However, as evident by the ability of larger dextranes to diffuse into the hydrogel (Figure 1), the distribution of mesh sizes is relatively broad with maximal mesh sizes $< \xi >_{max}$ about fourfold higher than the average mesh size $< \xi >$ (Table 2).

With FRAP (fluorescence recovery after photobleaching) we measured the diffusion coefficients of monodisperse fluorescent dextrans of various radii in
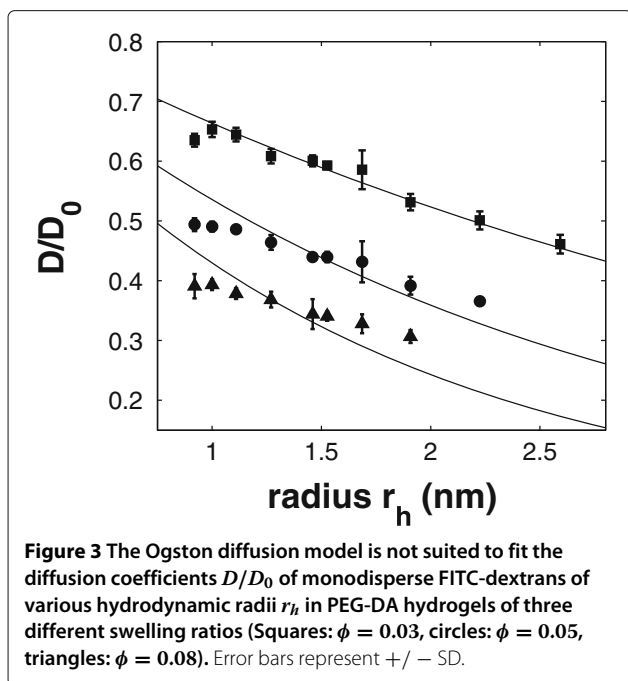
the PEG-DA hydrogels within seconds. For all dextranes no immobile fraction could be observed and the recovery of intensity within the bleached area could be easily fitted to determine the respective diffusion coefficient *D* in the hydrogel in respect to the diffusion coefficient in pure solvent D_0 (Figure 3). This indicates, that while the partitioning data deviates from our assumption that dextran is a neutral model diffusant, the probe particles do not remain entrapped, allowing us to characterize the gels based on the self-diffusion of the probe particles. The diffusion model of Ogston [23] predicts the diffusion coefficients of spherical molecules in a polymeric network of randomly oriented straight fibers by the equation

$$\frac{D}{D_0} = exp\left(-\frac{r_h + r_f}{r_f}\phi^{1/2}\right),\qquad(3)$$

where r_h represents the hydrodynamic radius of the diffusing species, r_f the polymer fiber radius and ϕ the polymer volume fraction. For the fitting analysis we used r_f as a free fitting parameter and for ϕ we used the values as they were calculated from the swelling ratio (see Table 1). For r_f we found 0.73 nm for $\phi = 0.03$, 0.56 nm

Table 2 Estimated average and maximal mesh sizes ξ of the PED-DA (20kDa) hydrogels for each polymer volume fractions based on polymer concentration *c*, elastic moduls *G* and parameter *s* obtained in the partition ratio analysis

ϕ	$< \xi >_c [nm]$	$< \xi >_G [nm]$	$< \xi >_s [nm]$	$\xi_{max} [nm]$
0.03	6.70 ± 0.45	4.80 ± 0.57	4.26 ± 0.16	16.3
0.05	5.60 ± 0.38	3.81 ± 0.58	2.07 ± 0.07	9.2
0.08	4.96 ± 0.33	3.44 ± 0.17	1.32 ± 0.07	6.8

Figure 3 The Ogston diffusion model is not suited to fit the diffusion coefficients D/D_0 of monodisperse FITC-dextrans of various hydrodynamic radii r_h in PEG-DA hydrogels of three different swelling ratios (Squares: $\phi = 0.03$, circles: $\phi = 0.05$, triangles: $\phi = 0.08$). Error bars represent $+/-$ SD.

Figure 4 Diffusion coefficients of FITC-dextrans in PEG-DA (20kDa) hydrogels at three different swelling ratios (Squares: $\phi = 0.03$, circles: $\phi = 0.05$, triangles: $\phi = 0.08$) do not deviate considerably at different temperatures (filled symbols: $T = 25°C$, open symbols: $T = 37°C$). Linear fitting analyses based on equation (4) are shown for the data measured at $T = 25°C$. Error bars represent $+/-$ SD.

for $\phi = 0.05$ and 0.48 nm for $\phi = 0.08$, in good agreement with the radius of a PEG fiber with a monolayer of bound water molecules ($r_f = 0.51$ *nm*) [24]. From the fitting analysis with Ogstons diffusion model it can be seen that for the lowest polymer volume fraction the fitting curve is in very good agreement with the diffusion data, whereas at both higher volume fractions the fitting curves loose agreement with the data. Other diffusion models that we found in the literature [10] were not able to further explain the diffusion measurements. There are several theories dealing with tracer diffusion in polymer solutions and crosslinked gels (reviewed in [10]). The diffusion is hindered by the obstruction caused by the polymer matrix, either by purely a steric hinderance or also through hydrodynamic interaction between the chains and the diffusant in the simplest cases (i.e. neglecting further interactions), or describing the gel as an effective medium. Most often the models employed to interpret the data contain exponential or Gaussian like functions to describe changes of the diffusion coefficient D/D_0 on the volume fraction and the size (hydrodynamic radius) of the diffusant. However, for low ϕ and r_h values they show very similar results, and often can be approximated with lower order (linear or parabolic) terms [25]. Analyzing our data we found a linear equation in the form (4) describes our data the best:

$$\frac{D}{D_0} = 1 - \alpha \cdot \phi - \beta \cdot r_h \tag{4}$$

(Figure 4), which is a form similar to the effective medium model of Giddings et al. truncated to the linear terms
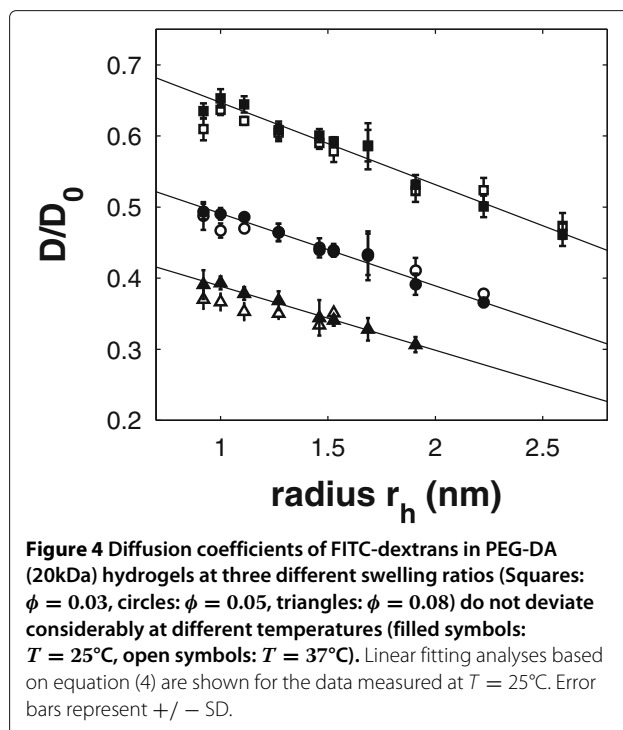
of the tracer size r_h [25]. Equation (4) relates the diffusion coefficients with the polymer volume fraction ϕ and the hydrodynamic radius of the diffusing molecules in the form of a master equation. The fitting parameters α and β are summarized in Table 3 for the three different swelling ratios. For α we found values between 6.9 and 7.8 and β lies between 0.09 and 0.12 nm^{-1}, both fit parameters show good agreement with one another for the different swelling ratios.

In order to investigate the influence of the temperature on the diffusion behavior the same measurements were repeated at a second temperature, T = 37°C. On the one hand the temperature influences the thermodynamic fluctuations of the polymer chains in the network that may influence the diffusion behavior, on the other hand the viscosity of water decreases by around 30% due to the temperature change allowing to investigate viscosity effects on the diffusion behavior. Figure 4 shows the diffusion measurements at both temperatures. It can be

Table 3 Results of the fitting analyses of the diffusion coefficients with equation (4)

ϕ	α	β
0.03	7.8 ± 0.9	0.12 ± 0.02
0.05	7.8 ± 0.3	0.10 ± 0.01
0.08	6.9 ± 0.2	0.09 ± 0.01

Errors represent the confidence interval (95%) of the fitting analyses.

seen that the diffusion coefficients overlap for both temperatures within their error bars for all three swelling ratios indicating that neither polymer chain fluctuations nor unpredicted viscosity effects significantly influence the diffusion behavior in the measured temperature range.

Conclusions

It is well known that permeability as well as mechanical properties of radically cross-linked PEG hydrogels depend not only on the size of PEG-DA polymers, but also on the polymer concentration in the reaction mixture [26,27]. Well defined fluorescent molecules employed in partition ratio analysis are ideally suited to determine the long time permeability properties of hydrogels. Including FRAP measurements enables an estimation of the amount of immobile fractions and short time scale behavior of the solutes. Where the average mesh sizes estimated from the swelling ratio and elastic moduli of the hydrogel correspond very well to values reported in the literature for PEG membranes [15] and our values estimated by partition ratio analysis. These average mesh sizes define the overall structure of the hydrogel. On the other hand, the distribution of mesh sizes and especially the maximal mesh size within the gel caused for example by network defects [27] enhances the ability of large molecules and proteins to diffuse through the hydrogel, another important feature for biological applications. Here, our partition ratio analysis indicates a broad mesh size distribution with maximal values up to four times the average. Independet of the distribution of mesh sizes, the large enhancement factor indicates an increased and unexpected capacity for the reversible uptake of hydrophilic molecules by PEG hydrogels. In combination with their high biocompatibility this explains the good suitability of PEG hydrogels in drug delivery applications. This work also nicely demonstrates the impact of slight changes in the fabrication protocol and the necessity to determine the diffusion characteristics of each set of hydrogels individually.

Methods

Preparation of PEG-DA hydrogels

Polyethyleneglycol-diacrylate macromer of 20 kDa molecular weight (PEG-20k-DA) were synthesised as described earlier [6] and mixed with degassed PBS (phosphate-buffered saline, $pH = 7.4$) to final concentrations of 10%, 20% and 30% (v/v). Photoinitiator 2-hydroxy-4'-(2-hydroxyethoxy)-2-methylpropiophenon (Sigma-Aldrich, Deisenhofen, Germany) was dissolved at a concentration of 10% (w/v) in 70% ethanol and added at a concentration of 1% (v/v) to the polymerization mixtures. The polymerization mixtures were vortexed and subsequently degassed by centrifugation (5 min, 4.4 rpm), then cast to glass molds consisting of a bottom glass plate and a top quartz glass plate separated by a distance of 0.4 mm. Pho-

topolymerization was carried out by a VL-6.L UV-lamp (Vilber Lourmat, Eberhardzell, Germany) at 365 nm for 20 min. Before further use the hydrogels were swollen to equilibrium in PBS for at least 24 h.

Swelling ratio

The volumetric swelling ratio $Q = V_{polymer}/V_{gel}$ of the hydrogels was determined based on the weight of the fully swollen hydrogels, the weight of PEG-DA in the precursor solution and the density ρ of bulk PEG in the amorphous state (1.12 g/cm^3). Measurements were done in triplicates. Based on the swelling ratio and the molar mass M_r of the polymer ($20\,kDa \pm 4\,kDa$) we estimated a theoretical mesh size (also see Appendix):

$$< \xi > = \left(\frac{M_r}{x \cdot \phi \cdot \rho \cdot N_A} \right)^{1/3} \tag{5}$$

Dextrans

In general, FITC (fluorescein isothiocyanate) labeled dextrans are produced commercially only by limited hydrolysis and fractionation. In order to obtain FITC-dextran samples of narrow size distribution and over a broad range of hydrodynamic radii further fractionation is required. We purchased FITC-dextrans with a mean molecular weight of 4 and 150 kDa (FD-4, FD-150S, Sigma-Aldrich, Deisenhofen, Germany). Fractionation allowed us to span a range of hydrodynamic radii between 0.9 and 12.2 nm (FD-150S dextrans have high polydispersity originally). This process was carried out by FPLC (fast protein liquid chromatography) fractioning on a HiPrep 26/60 Sephacryl S-300 high resolution column (GE Healthcare, Munich, Germany). FITC-dextrans were dissolved in PBS at a concentration of 50 mg/ml, sterilized by syringe filtration (Rotilabo syringe filter, 0.22 μm, Carl Roth GmbH, Karlsruhe, Germany) and degassed under vacuum for 30 min. After loading the column, the flow speed was set to 1.3 ml/min. Elution of FITC-dextran from the column was monitored at 280 nm and collected in fractions of 10/20 ml (FD-150S/FD-4). Each fraction was desalted by dialysis (3 repetitions of 4 h exposure to 2 l water baths of double distilled water using dialysis membranes of 1000 Da molecular weight cut-off (Spectra/Por Dialysis Membrane MWCO 1000, Spectrum Laboratories Inc., USA)) and subsequently freeze-dried (lyophilization). The hydrodynamic radii of the FITC dextrans in each of the fractions was determined by measurement of the diffusion coefficients using FRAP (fluorescence recovery after photobleaching, see section Translational diffusion measurements) and using the Stokes-Einstein relation. One of the fractions from the center of the distribution of the FD-150 polymer was fractionated a second time and analyzed for the size distribution of a typical fraction. Thus we measured the polydispersity index (PDI) to be 1.009

indicating that we obtained monodisperse FITC-dextran fractions.

Measurement of partition ratios

Equilibrium partition ratios $K_i = c/c_0$, with i representing a specific dextran, c the concentration of molecules in the hydrogel phase at equilibrium partitioning, and c_0 the concentration in the bulk solution, were measured by incubating hydrogel samples in FITC-dextran solution (0.5 mg/ml, PBS) for 5 days at 37°C.

The partition ratio for a given hydrogel sample and a given dextran was determined by measuring the fluorescence intensity signal from the hydrogel sample, and from a second sample containing bulk solution only, on a microscope setup (DeltaVision System, Applied Precision, Isaquah, USA) equipped with a cooled CCD camera (Cool Snap HQ, Photometrics, Tucson, USA), using the FITC-fluorescence channel (excitation 490/20 nm, emission 528/38 nm) and using an exposure time of 100 ms. The fluorescence intensity was calculated as the mean of the pixel intensity values of the image section taken by the camera. A background image with the fluorescence light turned off was also acquired to correct for dark counts. The partition ratio was then calculated by normalizing the thickness of the hydrogel sample to that of the bulk solution sample, given by

$$K_i = \frac{I}{I_0}\left(\frac{d}{d_0}\right)^{-1} \tag{6}$$

with I and I_0 the fluorescence intensity of the hydrogel sample and the bulk solution after subtraction of dark counts, d and d_0 the thickness of the hydrogel sample and the bulk solution. Chambers for the bulk solution were made by two coverslips separated by double sided adhesive tape spacers of 0.4 mm thickness. Hydrogel samples were dried using paper tissue (Precision wipes), placed on a coverslip, surrounded by a ring of medium viscous silicone oil (Baysilone-Paste, GE Bayer Silicones, Germany) and capped by a second coverslip. The exact thickness of the equilibrium swollen hydrogels was measured on a rheometer (Kinexus, Malvern, UK) lowering the upper plate down to the gel contact point by setting the normal force to a very low value (0.1 - 0.2 N). Linearity of intensity vs. sample thickness in the measured range was verified measuring the signal of bulk solution samples of various thicknesses (see Supporting Information). Furthermore, we checked the linearity of the intensity vs. FITC-dextran concentration in the range of the analyzed intensities.

Translational diffusion measurements

To determine the diffusion coefficients based on FRAP experiments, we applied the method of Tsay and Jacobson, which is based on the spatial Fourier analysis of the fluorescence recovery images [28]. This method was shown to be applicable to thick hydrogel samples [29] and we adapted it to our setup. In contrast to conventional FRAP methods (e.g. direct photometric analysis [30]), this method is not sensitive to the generally confounding optical effects caused by out-of-focus light and scattering and absorption by the sample, thereby allowing to obtain accurate results from diffusion measurements in three-dimensional samples [29].

For the FRAP measurements the samples were placed on the stage of an inverted microscope (Olympus IX 70) of a Delta Vision System (Applied Precision, Isaquah, USA) equipped with a mercury arc lamp (Mercury Short Arc, HBO, Osram) providing epi-illumination and a Cool Snap HQ CCD camera (Photometrics, Tucson, USA). The illumination profile of the mercury arc lamp was adjusted to be as homogeneous as possible over the entire field of view (1024 × 1024 pixel). Bleaching during recovery was minimized by closing a shutter in between the acquisition of images. Several prebleaching images were acquired in order to correct for the nonuniform illumination profile. The excitation filter (490/20 nm) and the emission filter (528/38 nm) were selected for the use of fluorescein. Photobleaching was carried out by a short laser pulse of 30 ms duration provided by an optically pumped solid-state laser (OPSL, Sapphire 488/20, Coherent Inc., Santa Clara, USA) operated at 488 nm in the TEM00-mode which yields a radially symmetric, approximately Gaussian intensity profile. The laser power was set to 90% of the maximum output power (20 mW). The laser source module is coupled to an optical fiber guiding the laser light to the microscope setup. The beam profile is expanded by coupling of the output fiber coupler to a telescope (beam expander), and thereafter focused close to the back focal plane of the objective (10×, NA = 1.2) in order to generate a cylindrically beam shape in the specimen. Low spatial resolution was chosen as optimal to avoid measuring effects arising from local inhomogeneities.

Recovery images were stored at a rate which was adapted to the time span of the recovery process by the control PC of the microscope (softWoRx Imaging Workstation, Applied Precision, Isaquah, USA). Each FRAP image sequence was converted to 16-bit .tiff images and exported for Fourier transform analysis implemented in MATLAB 2009b.

The effects of the nonuniform illumination profile have been eliminated by processing the relative fluorescence intensity, $I_{rel}(x, y, t_i)$, defined as

$$I_{rel}(x, y, t_i) = \frac{I_i(x, y, t_i)}{I_0(x, y)} \tag{7}$$

where $I_i(x, y, t_i)$ is the fluorescence intensity at a specific position x and y detected by the CCD camera after a specific post-bleach time t_i, and $I_0(x, y)$ the pre-bleach intensity profile obtained by calculating the average pixel intensity out of three pre-bleach images. Both were corrected for dark counts and for the contribution arising from the detection of ambient light. To correct for bleaching during recovery the pixel intensity values of a 50×50 pixel area far away from the bleaching center of each image of the sequence, were averaged and used as a correction factor yielding the bleaching-corrected intensity profile $I_{corr}(x, y, t_i)$ defined as

$$I_{corr}(x, y, t_i) = \frac{\beta_0}{\beta_{t_i}} \cdot I_{rel}(x, y, t_i) \qquad (8)$$

where β_0 is the hereby obtained pre-bleach intensity and β_{t_i} the post-bleach intensity for the i-th post-bleach image. For Fourier analysis of the FRAP sequence, a square (220×220 pixels) covering the complete recovery process and centering the bleach spot was extracted from the whole image sequence. The width of the square was chosen to be optimal for both comprising the whole recovery process and for having minimal noise contributions. PEG hydrogels are isotropic systems. Therefore, in a plane which is focused by the microscope, the recovery of fluorescent molecules can be modeled by Fick's second law [31]

$$\frac{\partial c(x, y, t)}{\partial t} = D\nabla^2 c(x, y, t) \qquad (9)$$

where $c(x, y, t)$ is the concentration relative to the pre-bleach distribution. Solving equation (9) in Fourier space leads to the simple solution

$$C(u, v, t) = C(u, v, 0) exp[-4\pi (u^2 + v^2)Dt] \qquad (10)$$

where $C(u, v, t)$ is the two-dimensional Fourier transform with spatial Fourier frequencies u and v. $C(u, v, 0)$ is the Fourier transform calculated from the first post-bleach image [28]. In Fourier transform space,

$$\frac{I(u, v, t)}{I(u, v, 0)} = \frac{C(u, v, t)}{C(u, v, 0)} \qquad (11)$$

as $I(u, v, t) = C(u, v, t)OTF(uv)$ where OTF is the optical transfer function [29]. Combination of equation (10) and (11) leads to

$$\frac{I(u, v, t)}{I(u, v, 0)} = exp[-4\pi (u^2 + v^2)Dt] \qquad (12)$$

and allows to determine D by fitting an exponential decay curve (non-linear least-squares curve-fitting algorithm) to the decay of Fourier amplitudes obtained by discrete Fourier transformation of each intensity profile $I_{corr}(x, y, t)$ of the recovery sequence. For fitting analysis we used all Fourier frequencies for which $u, v \leq 2$, corresponding to the five lowest frequency values (see Supporting Information for further explanation). Higher Fourier components were excluded as the corresponding decay amplitudes were prone to scattering originating from noise fluctuations in the images. Correct adjustment of the FRAP analysis setup was verified by checking the overlap of the Fourier decay coefficients for all of the five lowest spatial frequencies with a test solution and, further, by measuring diffusion coefficients for three different FITC-dextrans in a series of water-glycerol mixtures of known viscosity and comparing the results to the diffusion coefficients obtained theoretically using the Stokes-Einstein relation (see Supporting Information). We also ensured that the results of the experiments were independent of the sample thickness in the range used and of the concentration in the measured concentration range.

Rheometry

Rheometry was performed on a rotational rheometer (Kinexus, Malvern Instruments, UK). For each concentration of PEG-DA three different samples were measured to determine G' and G''. For all of the gels, the complex shear modulus G^*, where $G^* = G' + iG''$ and $G = \sqrt{(G')^2 + (G'')^2}$, was dominated by G' as the viscous contribution G'' was negligible. In detail, a parallel plate geometry of 20 mm diameter (PP 20) and a solvent trap was used. Dried hydrogel cylinders were fixed between the plates by a normal force set to 0.2 N. For all hydrogel concentrations, an initial amplitude sweep with an oscillatory shear strain of increasing amplitude at a constant frequency of 1 Hz was performed to determine the range of linear response. Based on this test, G was measured at an amplitude set within the linear elastic regime at constant frequency set to 1 Hz.

Based on G, the swelling ratio Q and a characteristic constant C_n we estimated a theoretical mesh size (see Appendix):

$$< \xi >_G = l \sqrt{\frac{RT \cdot C_n \cdot \rho}{x \cdot M_r \cdot G \cdot Q}} \qquad (13)$$

Appendix
Mesh size estimation based on the polymerization protocol

During preparation, the PEG chains used have two binding sites on each chain. Estimating the number concentration of chains in the gel as follows:

$$c = \frac{x\rho}{QM_r} \qquad (14)$$

Where we used x as the number of binding for each chain, ρ is the original (not swollen) density of the polymer and M_r is the molar weight of the monomer. Then one can

estimate a crude segment size from the volume occupied by each chain as:

$$\xi = \left(\frac{1}{N_A c}\right)^{1/3},\tag{15}$$

where N_A is Avogadro's number.

Mesh size calculation from the elastic modulus

In order to estimate the mesh size of the swollen hydrogels, we focused on estimating the number of monomers between crosslinking points. Knowing the number of monomers n in such a segment, the mesh size can be estimated as:

$$\xi^2 \approx C_n n l^2,\tag{16}$$

where C_n is a characteristic constant, l is a monomer size, usually $C_n \approx 4$ and $l \approx 1.54\ nm$ for PEG.

Considering a crosslink density ρ_x in the hydrogel, one can estimate n as:

$$n = \frac{N}{N_r} = \frac{\rho V \phi}{M_r} \frac{1}{x \rho_x V} = \frac{\rho}{x M_r Q \rho_x},\tag{17}$$

where N denotes the number of monomers in the gel, estimated from the mass of the polymer in the gel, based on the density ρ, the volume fraction ϕ or the swelling ration Q of the polymer and the molar mass M_r of the monomer. N_r is the number of polymer segments, which is related to the number of crosslinking points $\rho_x V$ by a factor x. This factor depends on the type of the network: for polymers where only two chains are bound together $x = 2$, while for a cubic mesh where each node is connected to 6 neighbors, $x = 3$.

The crosslinker density ρ_x we can estimate using the elastic modulus G from the following equation [32]:

$$G \approx \rho_x RT\tag{18}$$

Here we neglect the modification factors relating the length of the polymer chain in its free state versus in the gel, which is usually close to 1 [32].

Combining equations 16, 17 and 18, we find:

$$\xi \approx l \sqrt{\frac{RT C_n \rho}{x M_r G Q}}\tag{19}$$

Table 4 The results of the fitting analyses of the partition ratio with equation (1)

ϕ	A	$s[nm^{-1}]$	R^2
0.03	2.9	0.70	0.993
0.05	7.8	1.45	0.995
0.08	23.1	2.28	0.990

Results of fitting equation 1

The results of the fitting analyses of the partition ratio with equation (1) are summarized in Table 4. For r_f we used the radius of a PEG chain with a monolayer of water molecules [16]. A and s were used as fitting parameters. For s we found values between 0.70 and 2.28 nm^{-1} and for A we found 2.9 for the gels with the highest swelling ration and 23.1 for the gels with the lowest swelling ratio. R^2 was very close to 1 for all fitting analyses.

Author details
[1]Department of New Materials and Biosystems, Max Planck Institute for Intelligent Systems Heisenbergstr. 3, 70569 Stuttgart, Germany. [2]CSF Biomaterials and Cellular Biophysics, Max Planck Institute for Intelligent Systems Heisenbergstr. 3, 70569 Stuttgart, Germany. [3]Department of Biophysical Chemistry, University of Heidelberg, Heidelberg, Germany.

References
1. Yoshida R, Okano T (2010) Stimuli-responsive hydrogels and their application to functional materials. Springer, New York
2. Qiu Y, Park K (2012) Environment-sensitive hydrogels for drug delivery. Adv Drug Deliv Rev 64: 49–60
3. Gerlach G, Guenther M, Sorber J, Suchaneck G (2005) Chemical and pH sensors based on the swelling behavior of hydrogels. Sens Actuators B: Chem 111: 555–561
4. Lee YJ, Braun PV (2003) Tunable inverse opal hydrogel pH sensors. Adv Mater 15(7–8): 563–566
5. Richter A, Klatt S, Paschew G, Klenke C (2009) Micropumps operated by swelling and shrinking of temperature-sensitive hydrogels. Lab Chip 9(4): 613–618
6. Aydin D, Louban I, Perschmann N, Blümmel J, Lohmüller T, Cavalcanti-Adam EA, Haas TL, Walczak H, Kessler H, Fiammengo R, Spatz JP (2010) Polymeric substrates with tunable elasticity and nanoscopically controlled biomolecule presentation. Langmuir 26(19): 15472–15480
7. Raeber GP, Lutolf MP, Hubbell JA (2005) Molecularly engineered PEG hydrogels: a novel model system for proteolytically mediated cell migration. Biophys J 89(2): 1374–1388
8. Amsden B (1998) Solute diffusion within hydrogels. Mechanisms and models. Macromolecules 31(23): 8382–8395
9. Hoffman A (2002) Hydrogels for biomedical applications. Adv Drug Deliv Rev 43: 3–12
10. Masaro L, Zhu XX (1999) Physical models of diffusion for polymer solutions, gels and solid. Prog Polymer Sci 24(5): 731–775
11. Gehrke SH, Fisher JP, Palasis M, Lund ME (2006) Factors determining hydrogel permeability. Ann N Y Acad Sci 831: 179–184
12. Netz PA, Dorfm"uller T (1998) Computer simulation studies on the polymer-induced modification of water properties in polyacrylamide hydrogels. J Phys Chem B 102(25): 4875–4886
13. Muhr AH, Blanshard J (1982) Diffusion in gels. Polymer 23(7): 1012–1026

14. Bal T, Kepsutlu B, Kizilel S (2013) Characterization of protein release from poly(ethylene glycol) hydrogels with crosslink density gradients. J Biomed Mater Res A
15. Cruise GM, Scharp DS, Hubbell JA (1998) Characterization of permeability and network structure of interfacially photopolymerized poly(ethylene glycol) diacrylate hydrogels. Biomaterials 19(14): 1287–1294
16. Zhang X, Yang D, Nie J (2008) Chitosan/polyethylene glycol diacrylate films as potential wound dressing material. Int J Biol Macromol 43(5): 456–462
17. Kopecek J (2009) Hydrogels: from soft contact lenses and implants to self-assembled nanomaterials. J Polym Sci Part A 47: 5929–2946
18. Bohrer MP, Patterson GD, Carroll PJ (1984) Hindered diffusion of dextran and ficoll in microporous membranes. Macromolecules 17(6): 1170–1173
19. Arrio-Dupont M, Cribier S, Foucault G, Devaux PF, d'Albis A (1996) Diffusion of fluorescently labeled macromolecules in cultured muscle cells. Biophys J 70(5): 2327–2332
20. Mazza D, Braeckmans K, Cella F, Testa I, Vercauteren D, Demeester J (2008) De Smedt SS, Diaspro A. A new FRAP/FRAPa method for three-dimensional diffusion measurements based on multiphoton excitation microscopy. Biophys J 95(7): 3457–3469
21. Schnitzer JE (1988) Analysis of steric partition behavior of molecules in membranes using statistical physics. Application to gel chromatography and electrophoresis. Biophys J 54(6): 1065–1076
22. Kotsmar C, Sells T, Taylor N, Liu DE, Prausnitz JM, Radke CJ (2012) Aqueous solute partitioning and mesh size in HEMA/MAA hydrogels. Macromolecules 45(22): 9177–9187
23. Ogston AG, Preston BN, Wells JD (1973) On the transport of compact particles through solutions of chain-polymers. Proc R Soc A Math Phys Eng Sci 333(1594): 297–316
24. Dalton PD, Hostert C, Albrecht K, Martin M, Groll J (2008) Structure and properties of urea-crosslinked star poly[(ethylene oxide)-ran-(propylene oxide)] hydrogels. Macromol Biosci 8(10): 923–931
25. Pluen A, Netti PA, Jain RK, Berk DA (1999) Diffusion of macromolecules in agarose gels: comparison of linear and globular configurations. Biophys J 77: 542–552. http://www.ncbi.nlm.nih.gov/pubmed/11203465
26. Watkins AW, Anseth KS (2005) Investigation of molecular transport and distributions in Poly(ethylene glycol) hydrogels with confocal laser scanning microscopy. Macromolecules 38(4): 1326–1334. http://pubs.acs.org/doi/abs/10.1021/ma0475232
27. Engberg K, Frank CW (2011) Protein diffusion in photopolymerized . poly(ethylene glycol) hydrogel networks. Biomed Mater 6(5): 055006. http://www.ncbi.nlm.nih.gov/pubmed/21873762. [Linear D/D0 vs. RH, PEG hydrogels, good arguments in discussion.]
28. Tsay T, Jacobson K (1991) Spatial fourier analysis of video photobleaching measurements. Principles and optimization. Biophys J 60(2): 360–368
29. Berk D, Yuan F, Leunig M, Jain R (1993) Fluorescence photobleaching with spatial fourier analysis: measurement of diffusion in light-scattering media. Biophys J 65(6): 2428–2436
30. Jain RK, Stock RJ, Chary SR, Rueter M (1990) Convection and diffusion measurements using fluorescence recovery after photobleaching and video image analysis: in vitro calibration and assessment. Microvasc Res 39: 77–93
31. Cussler EL (1997) Diffusion: mass transfer in fluid systems. Cambridge University Press, Cambridge
32. Anseth KS, Bowman CN, Brannon-Peppas L (1996) Mechanical properties of hydrogels and their experimental determination. Biomaterials 17: 1647–1657